Journal of Applied Remote Sensing

Building a consistent medium resolution satellite data set using moderate resolution imaging spectroradiometer products as reference

Feng Gao
Jeffrey G. Masek
Robert E. Wolfe
Chengquan Huang

SPIE

Building a consistent medium resolution satellite data set using moderate resolution imaging spectroradiometer products as reference

Feng Gao,[a,b] Jeffrey G. Masek,[b] Robert E. Wolfe,[b] and Chengquan Huang[c]

[a] Earth Resources Technology Inc., Annapolis Junction, MD 20701, USA
[b] NASA Goddard Space Flight Center, Greenbelt, MD 20771, USA
[c] University of Maryland, Department of Geography, College Park, MD 20742, USA

Abstract. Medium resolution (10-100m) optical sensor data such as those from the Landsat, SPOT, ASTER, CBERS and IRS-P6 satellites provide detailed spatial information for studies of ecosystems, vegetation biophysics, and land cover. While Landsat remains a cornerstone of medium resolution remote sensing, the ETM+ scan-line corrector failure in 2003 has highlighted the need for methods to integrate radiometry from multiple international sensors in order to create a consistent, long-term observational record. Such an approach needs to compensate for differing acquisition plans, sensor bandwidths, spatial resolution, and orbit coverage. Different processing approaches used in the calibration and atmosphere correction across sensors make integration even harder. In this paper, we propose a generalized reference-based approach to convert medium resolution satellite digital number (DN) to MODIS-like surface reflectance using MODIS products as a reference data set. This approach does not require explicit calibration and atmospheric correction procedures for individual medium resolution sensors, therefore minimizing the potential impact of those procedures due to among-sensor differences. Therefore, data in MODIS era from different sources such as Landsat TM/ETM+, IRS-P6 AWiFS, and TERRA ASTER can be combined for time-series analysis, biophysical parameter retrievals, and other downstream analysis. Our results from Landsat TM/ETM+ show that this approach can produce surface reflectance with a similar accuracy to physical approaches based on radiative transfer modeling with mean absolute differences of 0.0016 and 0.0105 for red and near infra-red bands respectively. The normalized MODIS-like surface reflectances from multiple sensors and acquisition dates are consistent and comparable both spatially and temporally with known trends in phenology.

Keywords: MODIS, Landsat, ASTER, CBERS, AWiFS, data fusion, relative atmospheric correction, surface reflectance

1 INTRODUCTION

Medium resolution (10-100m) optical satellite sensors provide a spatial resolution that is suitable for monitoring biophysical and land cover processes at local, regional and global scales [1] and have been used widely to detect environmental changes [2,3]. These systems include the Multi-spectral Scanner (MSS), Thematic Mapper (TM), and Enhanced Thematic Mapper plus (ETM+) on the Landsat series satellites, the High Resolution Visible (HRV), High Resolution Visible Infrared (HTVIR), and High Resolution Geometric (HRG) sensors on SPOT series satellites, the Advanced Wide Field Sensor (AWiFS) and Linear Imaging Self-Scanner (LISS) III sensors aboard Indian Remote Sensing Satellite (IRS) [4], the Charge Coupled Device (CCD) camera aboard China-Brazil Earth Resources Satellite (CBERS) [5], and the Advanced Spaceborne Thermal Emission and Reflection Radiometer (ASTER) [6] on the EOS/TERRA platform.

Received 10 Jul 2009; accepted 20 Apr 2010; published 26 Apr 2010 [CCC: 19313195/2010/$25.00]

The Landsat satellites have been providing earth observation data continuously since early 1970s, and form a cornerstone for medium spatial resolution remote sensing. Maintaining the continuity of Landsat-like data is a critical need within the Earth Science community [7]. However, the failure of the Scan-Line Corrector (SLC) mechanism on Landsat 7 in 2003 and increasing age of Landsat 5 have threatened this continuity. While a new Landsat Data Continuity Mission (LDCM) satellite is now scheduled to launch in the end of 2012, the difficulties in maintaining Landsat continuity have highlighted the need to combine the capabilities of existing international sensors to provide a more robust observational record [8]. Such an approach can also provide more frequent observations necessary for monitoring rapid vegetation phenological changes during the growing season.

However, combining satellite observations from different platforms and sensors is complicated by their intrinsic differences in band configuration, acquisition time, illumination and viewing geometry, and radiometric calibration procedures. Surface reflectance derived from sensor radiance should be the basis for combining data from different sensors because theoretically it is a physical measurement not affected by instrument calibration issues or atmospheric effects, and is often a preferred input for deriving high-level biophysical products such as leaf area index and surface albedo. It provides a consistent long term data record for an individual sensor and helps to reduce errors in land cover change detection caused by atmospheric effects [9, 10].

Atmospheric correction can be accomplished using a physical radiative transfer model or a purely empirical approach [9]. The physical approach requires a detailed atmosphere profile including aerosol optical depth, ozone and water vapor content. Empirical approaches rely on ground measurements or are based on some assumptions. For example, dark object subtraction (DOS) approaches assume the darkest objects in a scene converge to a predefined surface reflectance [11]. Relative radiometric correction approaches require pseudo invariant features (PIFs) and assume those features are spectrally stable over time [12-15]. However, these ground invariant features may be limited by atmospheric and land cover or phenology changes. An extension of relative radiometric correction is to use simultaneously acquired coarse resolution image as reference. Olthof et al. [16] normalized Landsat ETM+ scenes using the 10-day composite SPOT VEGETATION (VGT) data as reference and produced Landsat ETM+ mosaics for the Hudson Bay Lowlands and found that the radiometric accuracy of the mosaic products were similar to those achieved through the radiometric correction approach using PIFs from overlapping Landsat images.

Aerosol optical thickness (AOT) is a major input to physical approaches for atmospheric correction. Due to lack of in situ AOT measurements for every image acquisition, AOT needs to be retrieved from an image itself using in an operational atmospheric correction approach. Kaufman et al. [17] found that for dark dense vegetation (DDV), simple relationships exist between the surface reflectance in TM band 7 (mid-IR) and those of band 1 (blue) and 3 (red). The aerosol optical depth can be estimated based on the actual observed top-of-atmosphere (TOA) reflectance and the predicted surface reflectance for these targets. This approach has been used in the Moderate Resolution Imaging Spectroradiometer (MODIS) surface reflectance algorithm [18] and has been implemented in the Landsat Ecosystem Disturbance Adaptive Processing System (LEDAPS) for processing Landsat TM and ETM+ images [10]. Unfortunately, this approach can only be applied to sensors that have the blue or middle infrared bands necessary for retrieving AOT.

Table 1 lists the spatial resolution and bandwidths from Landsat TM/ETM+, ASTER, AWiFS and CBERS-2 CCD as compared to the MODIS instrument. Three medium resolution sensors (ASTER, AWiFS and CBERS) have similar bandwidths to the Landsat TM/ETM+ but all are wider than MODIS. However, the DDV AOT algorithm of Kaufman et al. can not be applied to these three sensors due to the lack of either blue band (ASTER and AWiFS) or mid-infrared band (AWiFS and CBERS) from the same sensor. Physical approaches to correcting atmospheric effects cannot be applied without additional aerosol information.

Even if satellite data could be atmospherically corrected by either a physical or empirical approach, surface reflectance from different sensors may still not be comparable due to intrinsic differences in sensor bandwidths or viewing and illumination geometries. One approach to making a consistent data set from multiple sensors is to normalize measurements from those sensors using a consistent data set. In this paper, we present a generalized reference-based empirical approach for converting medium resolution data product from digital number (DN) to a standard surface reflectance product and demonstrate its use for the medium spatial resolution data in MODIS-era. We use the globally available, consistent MODIS surface reflectance products as the reference. As opposed to a physically-based atmosphere correction approach (e.g. LEDAPS), this empirical approach is a relative correction and therefore the corrected surface reflectance is a kind of "MODIS-like" surface reflectance. It provides a way to standardize satellite data from different medium resolution sensors to one standard and thus allow continuous time-series analysis and land cover change detection. Our approach builds on a long history of regression-based image normalization procedures from the remote sensing literature [12, 14, 16], and provides a practical "operational" framework for merging information from multiple sensors. Here we first provide a detailed description of this approach. We then present the results on applying this approach to Landsat, AWiFS, and ASTER data sets and discuss the advantages and limitations of this approach.

Table 1. Bandwidths and spatial resolution of Landsat TM/ETM+, TERRA ASTER, IRS-P6 AWiFS , CBERS-2 CCD and MODIS.

Landsat TM/ETM+	**TERRA ASTER**	**IRS-P6 AWiFS**	**CBERS-2 CCD**	**TERRA/AQUA MODIS**
30 meters	15 m, 30 m	56 meters	20 meters	250 m, 500 m
B1: 0.45-0.52			B1: 0.45-0.52	B3: 0.459-0.479
B2: 0.53-0.61	B1: 0.52-0.60	B2: 0.52-0.59	B2: 0.52-0.59	B4: 0.545-0.565
B3: 0.63-0.69	B2: 0.63-0.69	B3: 0.62-0.68	B3: 0.63-0.69	B1: 0.620-0.670
B4: 0.78-0.90	B3: 0.76-0.86	B4: 0.77-0.86	B4: 0.77-0.89	B2: 0.841-0.876
B5: 1.55-1.75	B4: 1.60-1.70	B5: 1.55-1.70		B6: 1.628-1.652
B7: 2.08-2.35	Cover B5-B8			B7: 2.105-2.155

2 APPROACH

2.1 A Generalized Reference-Based Approach

The generalized reference-based approach uses empirical relationships to convert raw satellite measurements to surface reflectance or other target biophysical measurements. The empirical relationships are built at the MODIS resolution using MODIS surface reflectance products as the reference.

The basis of this approach is that homogeneous pixels of the same land cover type have the same surface reflectance regardless of patch size, and that the seasonal and bidirectional reflectance changes of those pixels should also be the same for different patch sizes given each land cover type does not split into two or more types (1 to n) during a short period. The relationship of each land cover type between acquisition date and target date remain approximately same for different resolution images [10, 19]. Therefore, the relationships built on the MODIS data and the aggregated medium resolution data can be applied to medium resolution data to produce surface reflectance at a target date (e.g. MODIS acquisition date).

As shown in the schematic diagram (Fig. 1), the medium resolution data is first precision registered and orthorectified, reprojected and resampled to the MODIS resolution. An unsupervised classification is applied to the medium resolution data. A majority spectral cluster type of each MODIS pixel based on medium resolution pixels is computed and also used as criteria to determine homogeneity of MODIS pixel. Relationships between medium resolution data and cloud-free MODIS surface reflectance for each cluster are then built using "pure" coarse-resolution homogeneous pixels. The pure pixel at MODIS resolution for each cluster type is determined by the predefined percentage of majority cluster (default >20%). Only cloud-free pixels on both MODIS and medium resolution image can be selected as samples. Statistical relations between surface reflectance and satellite DNs are first built on the coarse resolution pure samples for the same cluster type. These relations are then applied to the original medium resolution data and thus produce surface reflectance for medium resolution data. For small clusters (default <1% of total pixels) without enough good "pure" samples (default <15) to work on, or correlation between DNs and MODIS data for the cluster is worse than that from whole image, a global relation regardless of cluster type will be used as a backup.

Differing from traditional empirical approaches that need to measure surface reflectance on the ground, this approach takes ground "truth" from MODIS data. MODIS surface reflectance products remove the water vapor and aerosol effects using a physical approach and provide pixel level data quality. The high quality MODIS data represent one of the most accurate data records we achieved today, and are thus an appropriate data source to use as a reference data set. This approach is different from the normalization method by Olthof et al. [16] that used random pixels as samples. We used the cluster-based pure homogeneous pixels as samples; this allows our approach to be generalized and deal with various seasonal changes from different surface types and can be extended to other biophysical parameters.

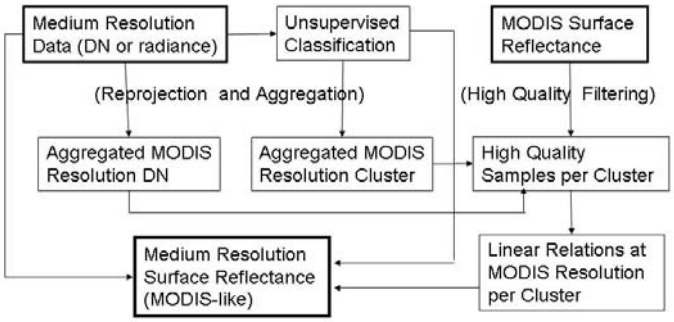

Fig. 1. Schematic diagram of the general empirical approach that corrects the medium resolution digital number (DN) to surface reflectance using MODIS surface reflectance as a reference data set.

2.2 Linear Correction Model

Empirical atmospheric correction approaches such as the dark object subtraction approach [11] and the radiometric rectification approach [12-14, 16] treat relations between DN and surface reflectance linearly. We also use a linear form to relate MODIS surface reflectance and medium resolution satellite DN for each cluster type. It can be expressed in:

$$y = a + b * x, \tag{1}$$

where y represents MODIS surface reflectance and x represents the aggregated digital number (DN) from the medium resolution image, and a and b are the intercept and slope. Note that only cloud-clear and "pure" homogeneous pixels are used to build relation for each cluster

type. If number of "pure" samples is less than predefined threshold, a global relation regardless of cluster type will be used as a backup.

Equation (1) allows converting DN to surface reflectance in one step without involving calibration process. It is a type of relative atmosphere correction since it uses MODIS surface reflectance as a reference. As opposed to most relative atmospheric correction methods, this approach relies on a MODIS observation instead of time-series pseudo invariant features (PIFs) that can be difficult to identify.

In Eq. (1), differences between MODIS and medium resolution data are unavoidable even if we strictly use high-quality MODIS observations and medium resolution data. Errors in medium resolution data (x coordinate) may be due to uncertainty in satellite sensor characteristics or preprocessing approaches. Variations in the MODIS surface reflectance (y coordinate) may be caused by sensor calibration and atmospheric correction. The theoretical accuracy of MODIS surface reflectance have been documented by Vermote [18, 20] as 0.005, 0.014, 0.008, 0.005, 0.012, 0.006 and 0.003 for seven MODIS land bands respectively (see Table 2).

Another source of errors comes from the geolocation uncertainty associated with matching observations from the two sensors. A pixel's footprint from two sensors cannot match exactly. The mismatching error can be reduced by decreasing spatial resolution as we assume surface reflectance is linearly scalable. However, reducing spatial resolution also reduces the dynamic data range of samples and may lead to less stable parameters in Eq. (1).

To consider errors in both coordinates, we adopted the merit function as defined in Press et al. (2007) for a general linear model.

$$\chi^2(a,b) = \sum_{i=0}^{N-1} \frac{(y_i - a - bx_i)^2}{\sigma_{yi}^2 + b^2\sigma_{xi}^2} \ , \tag{2}$$

where σ_{xi} and σ_{yi} are the standard deviations of *x* and *y* for the *i*-th point respectively. N is the total number of samples, and *a* and *b* are the intercept and slope for Eq. (1). The weighted sum of variances in the denominator is the variance of the linear combination $y_i - a - bx_i$ of two random variables x_i and y_i ,

$$Var(y_i - a - bx_i) = \sigma_{yi}^2 + b^2\sigma_{xi}^2 \ . \tag{3}$$

As Eq. (2) becomes nonlinear while searching minimum values of merit function with respect to *a* and *b*, a general non-linear minimization approach was used to determine a and b. We used a software package from Numerical Recipes in C [21] to solve this equation.

The choice of transform equation is totally depend on the relation of reference product and satellite DN value. A linear form is acceptable for surface reflectance when the satellite DN value is calibrated to at-sensor radiance [12]. A nonlinear form is more appropriate for some biophysical parameters such as leaf area index (LAI). Although each cluster uses a linear form to convert DN to surface reflectance, the overall conversion for whole image involves different clusters and thus is a nonlinear transformation. In this way, areas with different aerosol effects can be corrected using different equations if they are statistical separable in the unsupervised classification process.

2.3 Inputs from MODIS Products

The MODIS sensor aboard the Terra and Aqua platforms provides coarse resolution data products covering the period since 2000 for global-scale climate and ecosystem studies [22]. The MODIS land products provide information at spatial resolutions of 250, 500 and 1000

meters. MODIS surface reflectance is processed routinely, and pixel-based quality control information is associated with each product. The MODIS land products have been partially validated in "validated stage 1" [23]. The MODIS data processing algorithms are consistent in each data collection processing. The MODIS data products have been used in many applications since they are transparent, consistent, and freely available. For these reasons, we choose MODIS data as a reference in our study.

Three types MODIS surface reflectance products can be used as reference for our empirical model. They are the MODIS daily surface reflectance product (MOD09), the MODIS 16-day nadir Bi-directional Reflectance Distribution Function adjusted (BRDF-adjusted) surface reflectance (NBAR) (MOD43/MCD43) product, and the post-processed MODIS daily NBAR data (not part of the MODIS standard product suite).

The MODIS 500m daily surface reflectance product (MOD09GHK in collection 4 and MOD09GA in collection 5) can be used as a reference if viewing and solar geometries are similar to those for the medium resolution image. It corrects for the effects of atmospheric gases, aerosols and thin cirrus clouds [18]. The surface reflectance is retrieved from a radiative transfer model (Second Simulation of a Satellite Signal in the Solar Spectrum or 6S in short) using atmospheric inputs from NCEP (ozone, pressure) or directly derived the MODIS data (aerosol, water vapor). The surface reflectance product has been partially validated from a number of independent measurements and found approximately 90% of evaluated data are within the expected theoretical uncertainty [18, 20].

Though the MODIS daily surface reflectance provides high-quality surface reflectance at coarse resolution, the daily observations for any given location may be viewed from an off-nadir geometry and thus be affected by BRDF effects. The BRDF effects cannot be removed in the surface reflectance product for the medium resolution sensor produced by the general empirical approach. This may also lead to a higher uncertainty for the linear relation model. If timing is not a key in the application, a daily surface reflectance from a different day observed from nadir view (one every 16 days) is a possible substitute.

The second option is to use the MODIS 16-day NBAR product (1km MOD43B4 in collection 4 and 500m MCD43A4 in collection 5) as a reference data set. The MODIS NBAR product is computed from the MODIS BRDF parameters product based on the high-quality daily angular surface reflectance from each 16 day period [24]. The angular observations from each 16-day period are normalized to a nadir-viewing surface reflectance. In MODIS collection 5 processing, MODIS data from both the Terra and Aqua platforms are combined as inputs and BRDF products are produced at 500m resolution. The 8-day moving window approach was used in the production and thus there is a 16-day MODIS NBAR product for every 8-day period. The MODIS BRDF and NBAR products are also partially validated with independent measurements and shows good agreements with the field measurements [25]. Since the MODIS NBAR data exhibits relatively smooth seasonal trends, it was an input to product MODIS land cover product [26]. For applications that focus on seasonal and inter-annual changes, MODIS NBAR product is a good choice.

The third choice is to produce a MODIS daily NBAR data product as reference. Although not part of the standard MODIS product suite, the daily NBAR data can be produced from daily surface reflectance product and MODIS BRDF parameters by using the magnitude inversion approach. The magnitude inversion is a backup algorithm used in the MODIS BRDF/Albedo product. It takes BRDF shape as *a priori* information and adjusts BRDF curve to the observed bi-directional reflectance [24]. For daily NBAR, the magnitude inversion approach can be simplified as

$$\rho(\theta_i, \theta_v = 0, \varphi) = f(\theta_i, \theta_v = 0, \varphi, P) * \frac{\rho(\theta_i, \theta_v, \varphi)}{f(\theta_i, \theta_v, \varphi, P)}, \quad (4)$$

where θ_i, θ_v and φ are the illumination zenith angle, viewing zenith angle and relative azimuth angle respectively. $\rho(\theta_i, \theta_v, \varphi)$ is the daily bi-directional surface reflectance. $f(\theta_i, \theta_v, \varphi, P)$ is the computed bi-directional reflectance from the MODIS semi-empirical BRDF model. *P* represents the BRDF parameters from MODIS product. The nadir viewing reflectance satisfies the condition of $\theta_v = 0$. The bidirectional reflectance from MODIS BRDF parameters can be computed with

$$f(\theta_i, \theta_v, \varphi, P) = P_{iso} + P_{vol} * K_{vol}(\theta_i, \theta_v, \varphi) + P_{geo} * K_{geo}(\theta_i, \theta_v, \varphi), \quad (5)$$

where P_{iso}, P_{vol} and P_{geo} are the MODIS BRDF parameters for isotropic, volumetric and geometric scattering respectively. $K_{vol}(\theta_i, \theta_v, \varphi)$ and $K_{geo}(\theta_i, \theta_v, \varphi)$ are the kernels for the volumetric and geometric scattering respectively. In the MODIS BRDF product, the volumetric scattering kernel is derived from a radiative transfer model by Ross [27] under the thick vegetation coverage condition, and the geometric scattering kernel is derived from a geometric optical model by Li and Strahler [28] under sparse vegetation conditions. The complete formulas for two kernels are documented in Lucht et al [29] and Schaaf et al. [24].

The BRDF effects associated with MODIS daily observations are obvious as illustrated in Figure 2a shows the composition of MODIS surface reflectance of tile h11v04 acquired on April 26, 2006. In Fig. 2b, view zenith angle varies from 0 to 65 degrees. This tile is composed from two separate MODIS orbits. The BRDF effects are obvious from backward scattering (under the diagonal break line) to forward scattering (up the diagonal break line) within this MODIS image. We corrected the MODIS daily surface reflectance to daily NBAR using MODIS BRDF parameters during same period. Figure 2c shows the composition of the corrected daily NBAR data. The BRDF effects in Fig. 2c are reduced and differences around the diagonal break line disappear.

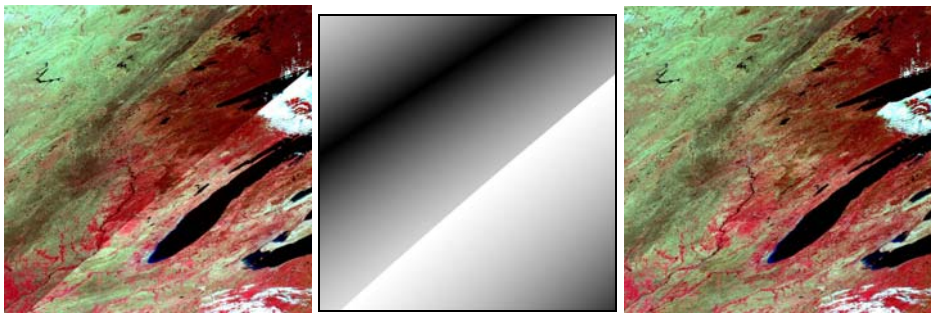

(a) daily surface reflectance (b) viewing zenith angle (c) daily NBAR

Fig. 2. MODIS daily surface reflectance (a) of tile h11v04 on April 26, 2006, the viewing zenith angle (b) (0 to 65 degrees) and the corrected daily NBAR (c).

This third option for MODIS reference data allows capture of daily variation in surface conditions and thus is appropriate for applications requiring daily revisit, such as crop growth monitoring. However, the separate step of processing and the fact that the off-nadir view has a larger foot print (at 55 degree off-nadir view, a MODIS pixel may be as large as 1km by 2km compared to the nadir view size of 0.5 by 0.5 km) may cause larger uncertainty of

surface reflectance. Thus the MODIS samples need to be aggregated to an even coarser resolution than original 500 meters.

2.4 Unsupervised Classification and Optional Spatial Aerosol Information

Unsupervised classification approaches bin continuous values into clusters based on their statistical distributions. We used the Iterative Self-Organizing Data Analysis Technique (ISODATA) to map spectral clusters in the medium resolution imagery. These clusters can then be related to "pure" (homogenous) observations at the MODIS resolution using the linear model in Eq. (1). The ISODATA classifier splits and merges clusters iteratively until classification conditions (e.g. number of classes or number of iteration) are satisfied. Note that the same surface type located in areas with significant differences in atmospheric conditions can be separated into different clusters. This ensures that different models (e.g. linear equation in this paper) can be applied under different atmospheric conditions and thus eliminate some effects caused by varying aerosol distribution.

The cluster map is also useful to determine the homogeneity of a coarse resolution cell by checking the percentage of a dominant cluster in a coarse resolution cell. Though the relations between surface reflectance and DNs are spatially scalable under uniform atmospheric condition, some biophysical parameters are not. It's critical to use pure homogeneous MODIS pixels as samples for those biophysical parameters and thus allow the relation built on the coarse resolution products to be extended to the original medium resolution image.

For a large area with varying aerosol distribution, additional aerosol information is helpful. Our approach does not require an actual aerosol optical depth. A relative variation map that distinguishes different levels of aerosol loading is sufficient. A linear relationship can be established for individual regions with homogenous aerosol loadings and applied to those regions based on the aerosol distribution map.

3 RESULTS AND ANALYSIS

3.1 Landsat ETM+ Surface Reflectance

The Terra MODIS crosses the equator at about 10:30AM local solar time, roughly 30 minutes later than Landsat 7. Their orbital parameters are identical, and as such the viewing (near-nadir) and solar geometries are close to those of the corresponding Landsat acquisition. This allows us to direct use MODIS daily surface reflectance (first input option) as a reference for Landsat 7 ETM+ data normalization.

Fig. 3 shows a Landsat ETM+ scene covering the Washington, D.C. area (WRS-2 path 15 and row 33) acquired on October 5, 2001. Since this Landsat scene is located in the MODIS tile boundary, several MODIS tiles are required to cover this Landsat scene. The MODIS 500m daily surface reflectance product (MOD09GHK) was first mosaiced and re-projected to the same projection and extent as the ETM+ scene (Fig 3a). The MODIS 1km daily state file (MOD09GST) was used to filter out clouds and cloud shadows. Only high-quality and clear surface reflectance values are reserved for creating the linear regression. Figure 4 shows the relationship between Landsat DN and MODIS surface reflectance at 1km resolution for red (a) and NIR (b) respectively. Spatial resolution has been rescaled from 500m to 1km to reduce variations from geolocation and resampling errors. Good linear relations for red and NIR can be seen in Fig. 4. The low values in the scatter plot for the red band (mostly water) (Fig. 4a) show different trends compared to the high values (mostly land). The different atmospheric effects and sensor spectral responses over water and land may cause this discrepancy. This can be partially solved in our approach by using different correction equations for water cluster. Figure 3b shows the converted Landsat ETM+ surface reflectance using our empirical approach and linear equation with merit function in Eq. 2. As ETM+

scene was acquired on the same MODIS acquisition (target) date, land cover changes can be neglected and thus the requirement for the cluster based correction can be relaxed or removed. In Fig. 3b, we used a high threshold (> 95% of majority cluster in MODIS pixel) to ensure that only good "pure" MODIS samples are applied for large clusters. For small clusters without enough "pure" samples to work on or correlation is not significant, a global relation regardless of cluster type was used. The same threshold was used in this paper when acquisition dates for medium resolution data and MODIS data are same.

To compare with surface reflectance derived from physical approach, we also computed ETM+ surface reflectance using the LEDAPS approach (Fig. 3c). The LEDAPS was developed to create a Landsat-based surface reflectance product for North America to support the North American Carbon Program (NACP) [10]. It adopts the MODIS atmospheric correction approach for Landsat TM and ETM+ data, with aerosol thickness derived from the imagery itself. As LEDAPS uses the same "6S" approach for Landsat atmospheric correction, uncertainties for Landsat and MODIS surface reflectance are comparable [10]. Figure 3b and 3c shows very similar surface reflectance composited from near-infrared, red and green bands with same stretches.

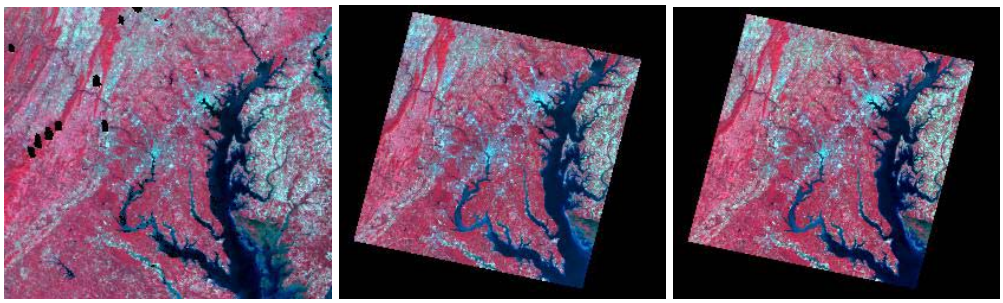

(a) MODIS (b) empirical approach (c) LEDAPS

Fig. 3. MODIS surface reflectance (a) and Landsat ETM+ surface reflectance derived from the reference-based approach (b) and LEDAPS physical approach (c) for Washington DC area (Landsat WRS-2 path 15 and row 33). Black areas represent clouds, cloud shadows, missing or poor quality data that can not be selected as a sample. All images are shown in same projection and extent.

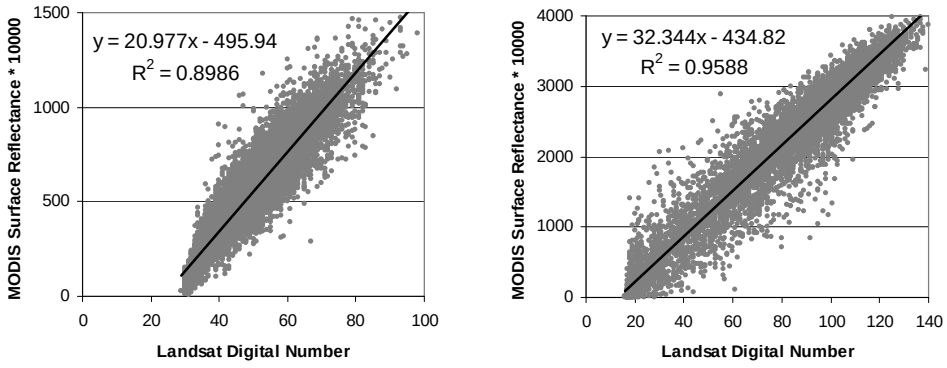

(a) red (b) NIR

Fig. 4. Scattering plots of Landsat digital number and MODIS surface reflectance (*10000) for red (a) and NIR (b) respectively.

The differences of Landsat ETM+ surface reflectance from the reference-based approach and the LEDAPS approach are further compared with mean difference and mean absolute difference. In the comparison, we use d(r1,r2) to represent the mean difference between reflectance r1 and r2 and use ad(r1, r2) to represent the mean absolute difference between r1 and r2.

Table 2 shows the mean absolute difference and mean difference among the MODIS surface reflectance, Landsat ETM+ surface reflectance from our empirical approach and Landsat ETM+ surface reflectance from the physically-based LEDAPS approach. The comparison between MODIS and Landsat surface reflectance is evaluated at the spatially aggregated MODIS resolution (1 km for this table). The comparison of Landsat ETM+ surface reflectance from our empirical approach and LEDAPS is evaluated at the original ETM+ resolution (28.5 meters). Table 2 shows that the differences between general empirical approach and LEDAPS approach (d(g,l) and ad(g,l)) are very small. The mean difference between empirical approach and LEDAPS approach are 0.0007and -0.0102 for red and NIR band respectively, which is smaller than the theoretical accuracy of MODIS surface reflectance itself (0.0050 for red and 0.0140 for NIR). The mean differences of surface reflectance between MODIS and ETM+ with general empirical approach (d(m,g)) are neglectable, which means the differences between empirical approach and LEDAPS approach (d(g,l) and ad(g,l)) are mainly due to the intrinsic differences between MODIS and LEDAPS surface reflectance (d(m,l) and ad(m,l)). The large mean absolute differences between MODIS and ETM+ empirical surface reflectance (ad(m,g)) are due to the bandwidth differences and geolocation/resampling errors. However, the merit function (Eq. 2) still produced a very good fit (negectable d(m,g)) given enough high quality samples are maintained.

Table 2. Mean absolute difference (ad) and difference (d) among MODIS (m) and Landsat surface reflectance from the reference-based approach (g) and LEDAPS (l) (MODIS theoretical accuracy for surface reflectance is listed as MODIS_TA for similar ETM+ bands).

ETM+	**Band 1**	**Band 2**	**Band 3**	**Band 4**	**Band 5**	**Band 7**
d(m, l)	-0.0075	0.0012	0.0005	-0.0093	0.0141	-0.0011
d(g, l)	-0.0075	0.0004	0.0007	-0.0102	0.0156	0.0001
d(m, g)	0.0000	0.0007	-0.0004	0.0002	-0.0020	-0.0014
ad(m, l)	0.0080	0.0045	0.0054	0.0157	0.0177	0.0088
ad(g, l)	0.0078	0.0024	0.0016	0.0105	0.0156	0.0005
ad(m, g)	0.0053	0.0056	0.0069	0.0139	0.0138	0.0105
MODIS_TA	0.0080	0.00050	0.0050	0.0140	0.0060	0.0030

A strong linear relation between the empirical and LEDAPS surface reflectance values can be also seen from the scatter plots in Fig. 5. However, the relationship deviates from the exact 1 to 1 line. This implies that the Landsat ETM+ surface reflectance from empirical approach may not precisely duplicate the true Landsat surface reflectance. Instead it generates a MODIS-like surface reflectance, corrected to replicate the MODIS spectral bandpasses.

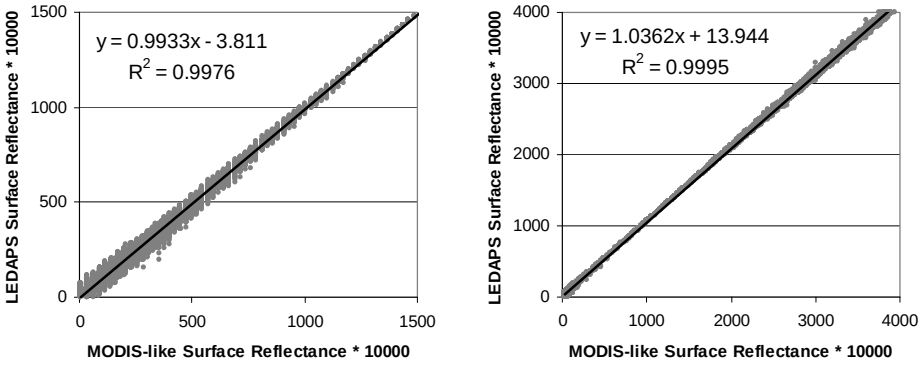

(a) red (b) NIR

Fig. 5. Scattering plots of Landsat surface reflectance from the reference-based approach (MODIS-like) and LEDAPS approach for red (a) and NIR (b) respectively.

3.2 AWiFS Surface Reflectance

The AWiFS camera on the IRS-P6 (India ResourceSat) consists of two electro-optic modules (AWiFS-A and AWiFS-B) which provide a combined swath width of 740 km. It provides four spectral bands with 10 bit radiometric resolution and 56m nadir spatial resolution [30]. Given its frequent (4-5 days) revisit cycle and wide swath (740 km), AWiFS data are very useful for large area applications. In fact, the USDA National Agricultural Statistics Service (NASS) selected AWiFS data for their development of the 2006 Crop Data Layer [31].

While Landsat 7 ETM+ flies the same orbit as Terra MODIS, IRS-P6 AWiFS has different orbital path and thus different viewing geometries for the same location even though the satellite overpass times are nearly identical (10:30AM local time at the equator). The direct use of MODIS daily surface reflectance (first option) or MODIS NBAR data (second option) as the surface reference may limit the ability to detect daily surface changes. The BRDF corrected daily NBAR data (third option) is considered as a reference data set to correct AWiFS DN to surface reflectance in our test.

The BRDF corrected MODIS daily NBAR data in Fig. 2c was used as the reference data set. Figure 6a shows the subset of the daily NBAR data on April 26, 2006. Figure 6b is the same day AWiFS surface reflectance produced by general empirical approach. Figure 6c shows the same day Landsat TM surface reflectance produced by empirical approach using same MODIS daily NBAR data as reference. The surface reflectance from Landsat TM and AWiFS look very similar visually in Fig. 6. The scatter plots between AWiFS and TM surface reflectance (Fig. 7) show that they agree closely. Table 3 shows the mean difference and the mean absolute difference between AWiFS and TM surface reflectance produced by our empirical approach. The differences between the two surface reflectance data sets are very small. Those differences may due to the discrepancy between the relative spectral response of AWiFS and TM [32] or a mismatch in the pixel's footprint between the two sensors.

Table 3. Mean absolute difference and difference between AWiFS and TM surface reflectance from the reference-based approach (aggregated to 112m resolution for comparison).

AWiFS/TM	**Band 2**	**Band 3**	**Band 4**	**Band 5**
Mean diff.	-0.0009	-0.0015	0.0007	-0.0012
Mean abs. diff.	0.0022	0.0056	0.0087	0.0108

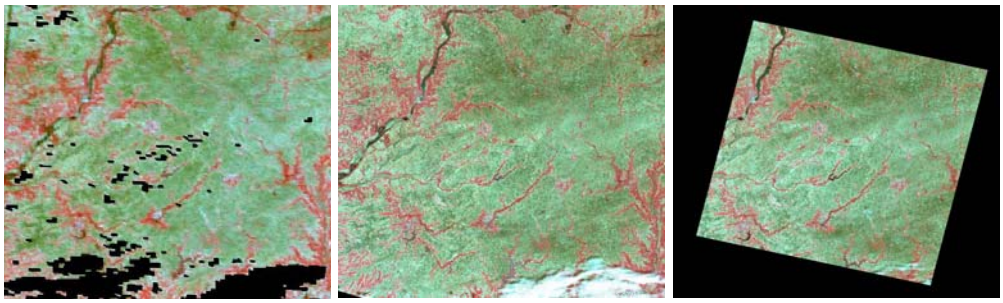

(a) MODIS (b) AWiFS (c) Landsat TM

Fig. 6. The MODIS daily NBAR (a), Landsat TM surface reflectance (b) and AWiFS surface reflectance (c) both corrected by the reference-based approach show similar color and spatial patterns. Black represents missing or poor quality data. All data were acquired on April 26, 2006.

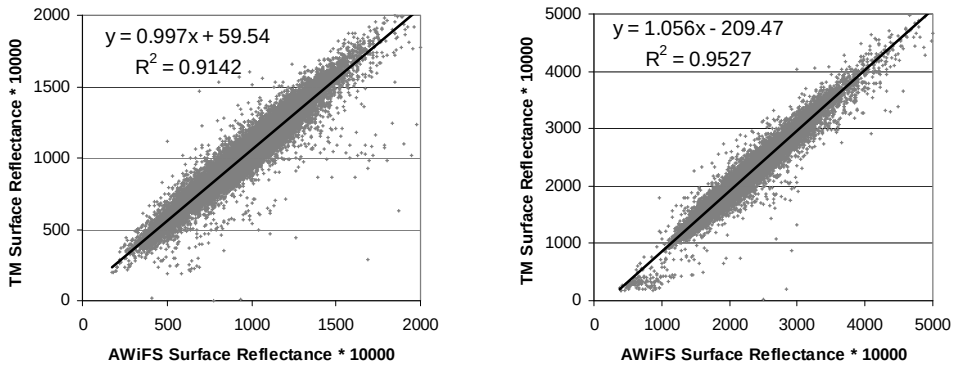

(a) red (b) NIR

Fig. 7. Scattering plots of AWiFS surface reflectance and Landsat TM surface reflectance in red (a) and NIR (b) band.

3.3 Combining ASTER Scenes from Different Acquisition Dates

Compositing satellite images from different acquisition dates are a challenge for medium spatial resolution data, especially when the satellite images are acquired from different seasons [33]. Using our approach, medium spatial resolution images from different acquisition dates can be normalized to a close and clear MODIS acquisition date in MODIS-like surface reflectance. Figure 8 illustrates the processing result over central Virginia. In the test, we used ASTER scenes that were acquired from Fall 2005 to Spring 2006 (10/23/05, 11/10/05, 1/27/06 and 4/10/06) and a MODIS image acquired on 4/10/2006. As three ASTER scenes (10/23/05, 11/10/05 and 1/27/06) were acquired from different MODIS acquisition date (4/10/06), the changes of vegetation phenology or land cover need to be considered. We used low threshold (> 50% of majority cluster in MODIS pixel) to extract "pure" samples and thus allow more clusters being processed with their specific cluster-based relations. Figure 8(a) shows a map stitched from original L1B ASTER data with different acquisition dates (b). The differences of seasonality/BRDF are obvious on this map. However, those differences have been reduced in the mosaic map (d) of the BRDF/seasonality corrected ASTER images by using MODIS surface reflectance (c) as a correction reference. The remaining differences

between adjacent ASTER paths may reflect diverging land cover conditions through the growing season (e.g., same land cover on the ASTER acquisition date but different on the MODIS acquisition date thus causing a "1:n" non-function relationship). Results can be improved by using additional ASTER images to distinguish land cover types and avoid "1:n" relationship in models.

Figure 9 shows scatter plots of the normalized ASTER surface reflectance and Landsat ETM+ surface reflectance. Landsat ETM+ SLC-off data was acquired on the same day (April 10, 2006) as the MODIS target date. We used our reference-based empirical approach to produce Landsat ETM+ surface reflectance. We limited valid pixels in the comparison. In order to reduce the errors caused by the mis-registration, pixels from ASTER and Landsat are spatially averaged to the same coarser spatial resolution (60 m) for pixel-to-pixel comparison. Scatter plots in Fig. 9 show linear relations with r-squares of 0.642 and 0.721 for red and near-infrared bands respectively. The average absolute differences between ASTER and ETM+ surface reflectance are 0.0057, 0.0093, 0.0190, and 0.0212 for ASTER band 1(green), band 2(red), band 3(NIR), and band 4 (SWIR) respectively.

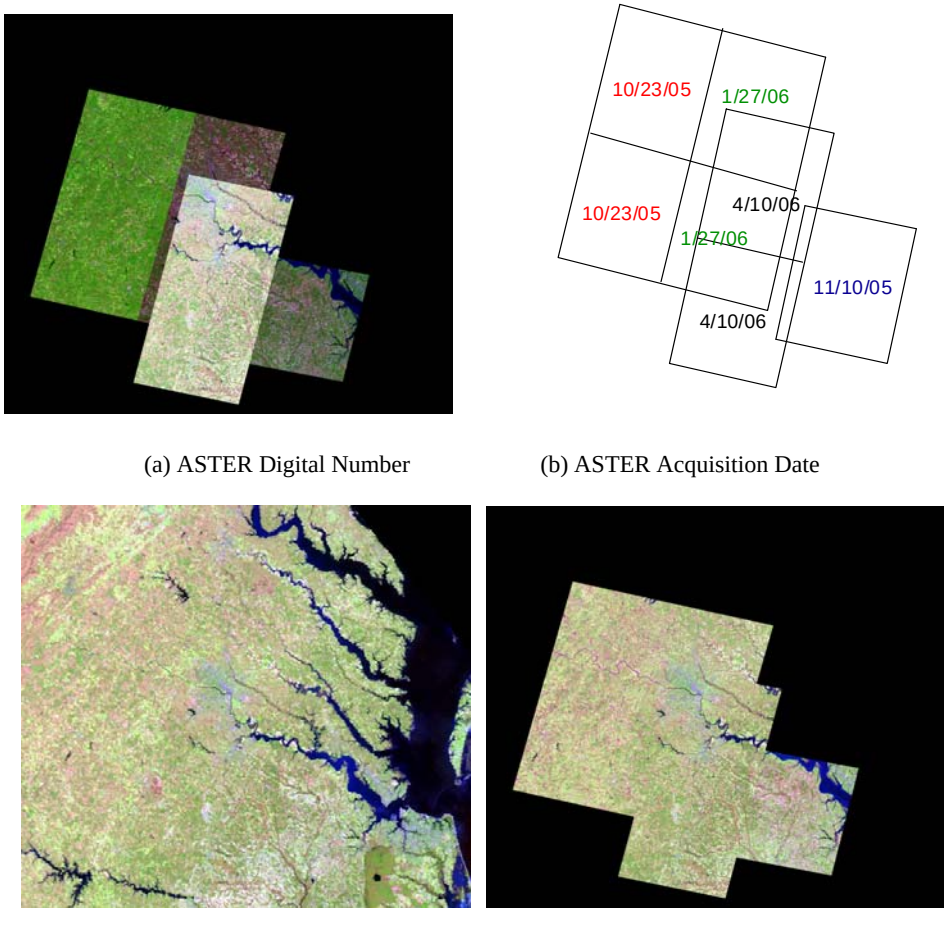

(a) ASTER Digital Number (b) ASTER Acquisition Date

(c) MODIS Surface Reflectance (d) Normalized ASTER Surface Reflectance

Fig. 8. Seven ASTER scenes in digital number (a) acquired from different dates (b) are normalized to the MODIS-like surface reflectance (d) by using a MODIS surface reflectance (c) acquired on April 10, 2006 as reference.

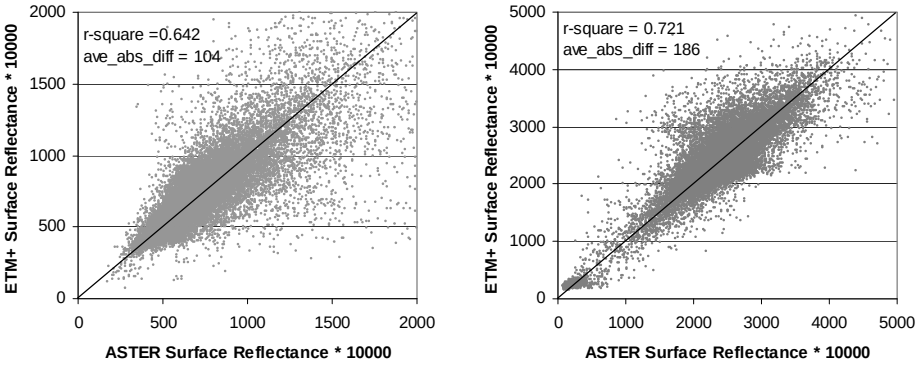

(a) red (b) NIR

Fig. 9. Scattering plots of the normalized ASTER surface reflectance and Landsat ETM+ surface reflectance in red (a) and NIR (b) band. The scattering samples are close to 1:1 lines (diagonal lines).

3.4 Combining Multiple Data Sources

The general reference-based empirical approach provides a way to combine different medium resolution data sources to produce a consistent surface reflectance record when MODIS surface reflectance is used as a reference data set. In this test, we mixed different medium resolution data for time-series analysis of crop phenology. Table 4 lists the available medium resolution data sources for our test site located in central Illinois. The medium resolution data sources include two ASTER scenes, two Landsat TM scenes, one Landsat ETM+ SLC-off scene and three AWiFS scenes. The MODIS daily surface reflectance product (option 1) is used as a reference data set if nadir view MODIS data is available (O1 in Table 4). Otherwise, the BRDF corrected daily NBAR (option 3) will be used instead (O3 in Table 4). The available data sources in Table 4 encompass the 2006 growing season for principal crops in the area. As multiple data sources need to be analyzed at one spatial resolution, all data sources have been co-registered, orthorectified and resampled to the coarsest spatial resolution (AWiFS at 56 m). Cloud masks for cloudy scenes (7/7/06 and 8/24/06) were created manually. Cloud masks should be aggressive and ensure only clear pixels are included as samples. Coarse resolution samples with partial coverage of medium resolution pixels due to clouds or missing are excluded from the selection.

Table 4. List of available data sources during growing season (O1 is the first option that uses MODIS daily surface reflectance and O3 is the third option that uses MODIS daily NBAR data).

Date	**4/18/06**	**4/26/06**	**6/5/06**	**6/13/06**	**7/7/06**	**7/23/06**	**7/31/06**	**8/24/06**
Sensors	ASTER	AWiFS	ASTER	TM	AWiFS	ETM+	TM	AWiFS
MODIS	O1	O3	O1	O3	O1	O1	O3	O1

Fig. 10 shows surface reflectance produced from four different medium resolution sensors during April to August, 2006. A continuous seasonal trajectory can be seen from the image time series. Different surface types show different green-up dates with peak greenness occurring in the image of July 31, 2006.

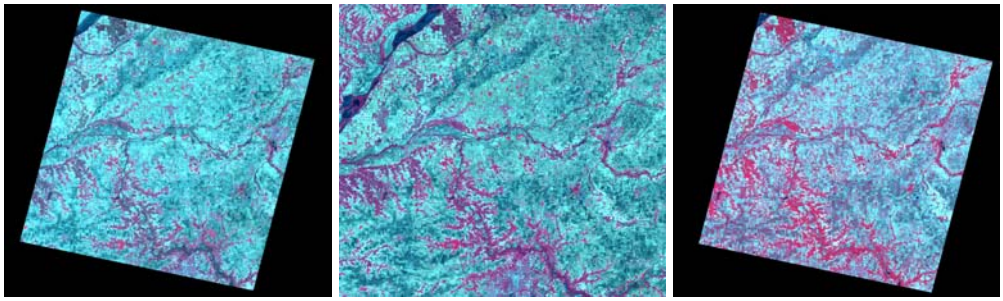

(a) 4/18/06, ASTER (b) 4/26/06, AWiFS (c) 6/5/06, ASTER

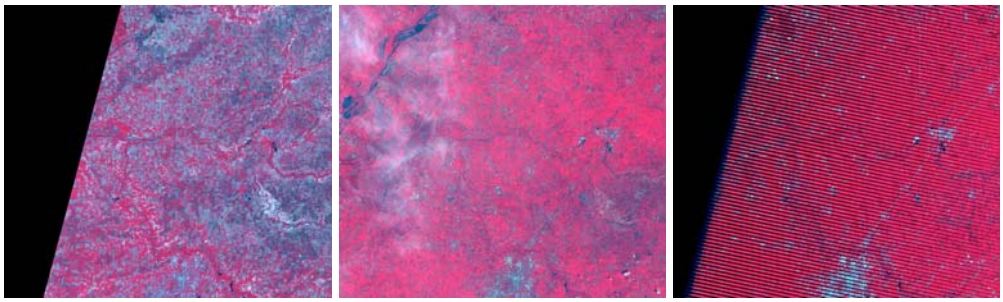

(d) 6/13/06, TM (e) 7/7/06, AWiFS (f) 7/23/06, ETM+

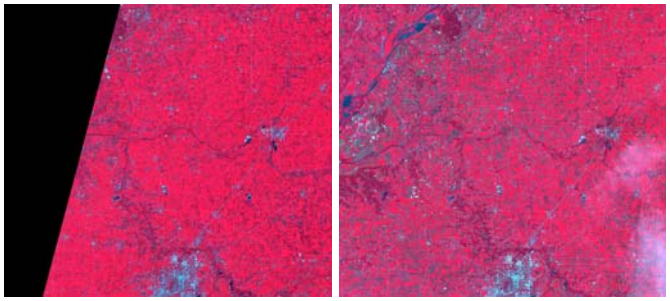

(g) 7/31/06, TM (h) 8/24/06, AWiFS

Fig. 10. Time series of surface reflectance produced by the reference-based approach from different data sources, shown using same RGB stretch (NIR: 0.1-0.5; red: 0.01-0.16; green: 0.01-0.12).

Using the derived time series, we show the seasonal spectral evolution of major vegetation types (Fig. 11) in central Illinois in Fig. 12. In this plot, natural vegetation types such as woods (sample 1) and pasture (sample 2) green up as early as April. Their reflectance and NDVI values tend to be less variable during this period. The dominant crop types (soybeans and corn) green up in early June and reach peak greenness in late July. The two corn samples show different seasonality in both reflectance and NDVI plots, which may due to the different surface conditions or misclassification in the 2006 Cropland Data Layer (CDL). The claimed accuracy of the crop type is around 85-95% [31]. The soybean sample shows a similar temporal pattern to one corn site (sample 4) in the NDVI plot (Fig. 12c). However, their surface reflectances are quite different for both red (Fig. 12a) and NIR (Fig. 12b) bands. Soybeans show a much higher surface reflectance (around 0.60) in the NIR band while corn

only reaches 0.45. The NDVI values for crops and woods are similar at peak greenness, which may due to the low surface reflectance in the red band which thus saturates the NDVI value. The time-series surface reflectance reveals more growth information than NDVI values alone.

We compute MODIS NDVI values of same locations from the 8-day 250m MODIS surface reflectance composite product. The MODIS NDVI data (lines in Fig. 12c) show consistent time-series trends compared to the medium resolution data from different sensors. The forest sample shows the best fit to the MODIS NDVI time-series. The pasture sample shows similar time-series trends but consistently lower NDVI values than MODIS except for the last date (8/24/06). Crop samples also show similar time-series patterns with very close values during full growth season but lower values in early season. This may be due to the fact that MODIS 250m pixels for these sample locations are not pure homogeneous pixels. A larger coverage area from MODIS off-nadir observation also affects the sample homogeneity. For mixtures of pasture and crops, the NDVI values during early growing season are partially contributed by forest pixels. Since forest samples are located in large continuous tracts, it is more likely to correspond to a homogeneous pixel in the MODIS image. The time-series NDVI data from the forest sample fits to multiple medium resolution data very well. Both MODIS time-series and multi-sensor medium spatial resolution data reflect the forest phenology changes during this period. This agreement supports that medium resolution data from different sensors can be combined for the time-series analysis using the reference-based empirical approach.

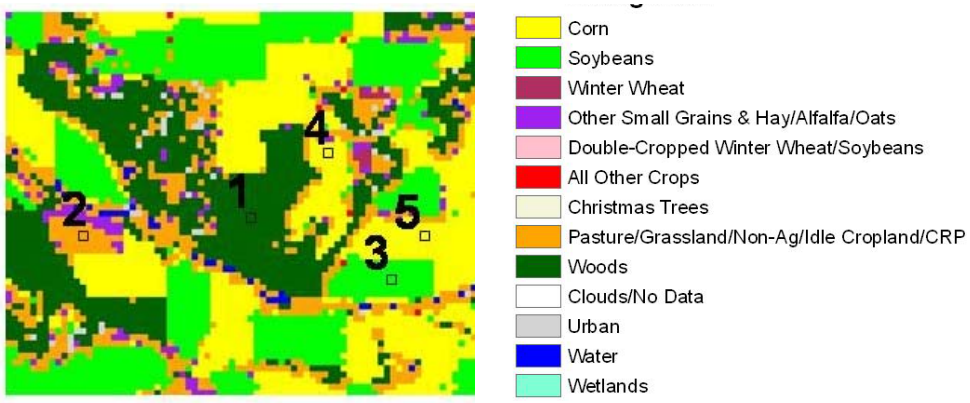

Fig. 11. Typical surface types in this area (central location: 40.094823N, 89.512883W) and sample locations from the USDA 2006 Cropland Data Layer (CDL).

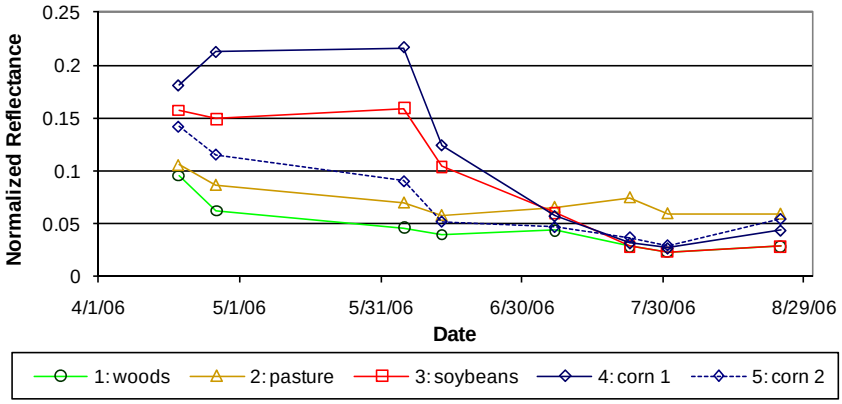

(a) red

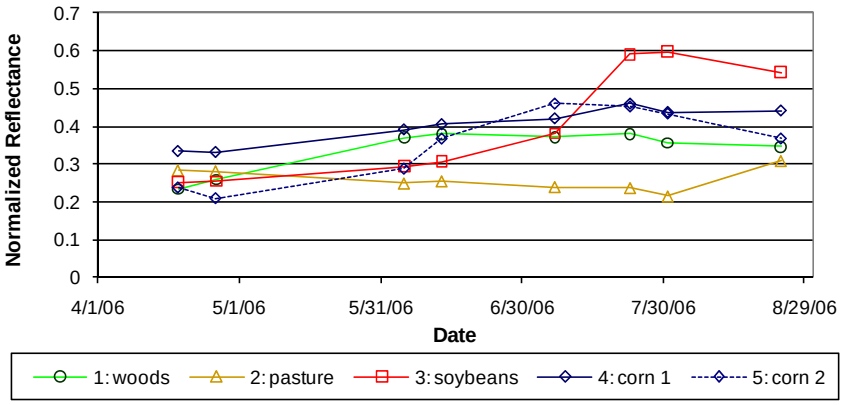

(b) NIR

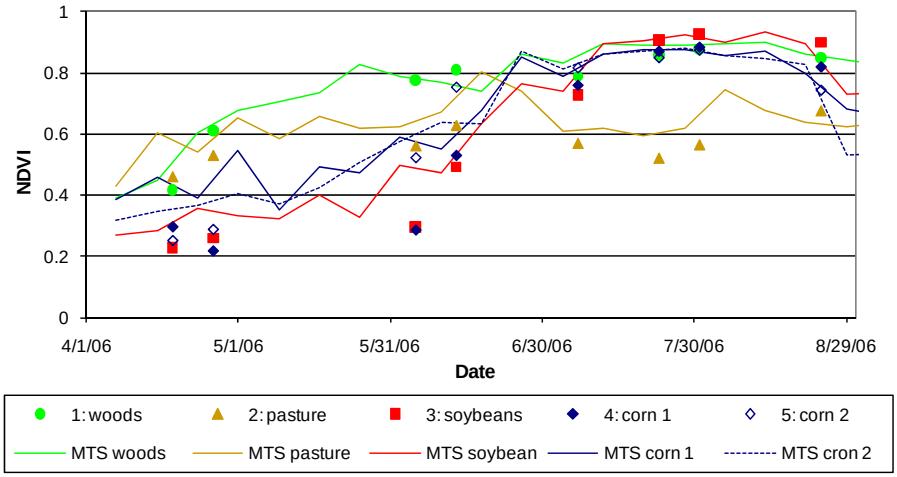

(c) NDVI

Fig. 12. Typical surface types in this area show seasonal variations of surface reflectance (a and b) and NDVI (c) for different samples from different data sources during April to August, 2006. The seasonal variations of NDVI (c) from medium spatial resolution sensors are consistent with the MODIS NDVI time-series (MTS).

4 DISCUSSION AND CONCLUSIONS

Medium spatial resolution (10-100m) satellite data are extremely useful for local and regional remote sensing applications. The scan-line corrector failure of Landsat 7 and the age of Landsat 5 threaten (like the recent rapid increase in Landsat 5's Traveling Wave Tube Amplifier (TWTA) helix current, which may cause the end of Landsat 5) the continuity of global medium resolution data archive before Landsat 8, or LDCM, starts to operate in December 2012. Though there are several mid-resolution data sources available, none of them can replace Landsat mission completely. However, combining these different medium resolution data sources can increase the frequency of observations, reduce the risk of a Landsat data gap, and enrich the global medium resolution data archive. The general reference-based approach proposed in this paper allows different data sources to be combined using one "standard" surface reflectance as a reference data set.

Comparing to other relative rectification approaches that reply on pseudo invariant features (PIFs), the reference-based approach can be applied to areas where PIFs are hard to find. However, as this is a reference based approach, its applications are limited by the reference data set. Different from the reference-based approach used by Olthof et al. (2005), this general reference-based approach can be applied to normalize scenes that contain different seasonalities from different surface types. The reference-based approach can not only normalize scenes acquired from different dates to one close target date but also can combine remote sensing data from different sensors for time-series analysis. However, this approach cannot be applied to the situation when same land cover (cluster) shows on the medium resolution image but changes on the MODIS acquisition date and cause a "1 to n" non-function relationship. For example, bare soil cluster in medium spatial resolution image may split to different crops (or stay as bare soil) in the MODIS target date, we will not able to make one function transformation between soil type (1) in medium spatial resolution image to multiple crops (n) in MODIS target image unless additional information is provided. Through we only demonstrate the general reference-based approach for surface reflectance using a series of simple linear functions, the approach can be extended to non-linear situations (such as leaf area index).

The MODIS reflectance products are the appropriate data sources for use as a reference due to unique characteristics of MODIS products: 1) MODIS has similar bandwidth to medium resolution data sources; 2) MODIS data products are consistent from each collection of processing; 3) MODIS provides daily global coverage data; 4) MODIS products have been validated in transparent validation exercises and provide comprehensive pixel level quality control flags and 5) MODIS products are freely available on-line and easy to access. There are three choices to use MODIS reflectance as a reference data set. One can use MODIS daily surface reflectance product or MODIS 16-day NBAR product directly. For the applications that need capturing variations on daily-basis, the BRDF effect corrected daily NBAR can be used as input. Though we only demonstrate MODIS data in this paper, other coarse resolution data products may be used as reference data set as well.

Though the generalized reference-based approach is simple, the results using Landsat ETM+ show it can still achieve similar accuracy compared to physically-based atmospheric correction approaches. The differences between the two approaches are mainly due to the intrinsic differences between MODIS and Landsat ETM+ surface reflectance. This approach works as a relative atmospheric correction approach when MODIS target date is the same as medium resolution data. The corrected surface reflectance is a MODIS-like value, corrected to MODIS band pass.

Different from other data fusion approaches such as the Spatial Temporal Adaptive Reflectance Fusion Model (STARFM) [34] and the Spatial Temporal Adaptive Algorithm for mapping Reflectance Change (STAARCH) [35], this approach only requires one target MODIS data and thus simpler and faster. However, it assumes that land cover types do not

change and split to 1:n relation between medium spatial resolution sensor and target MODIS acquisition date. Ideally, the medium spatial resolution data and MODIS data should be acquired from the same season in similar phenology stage. The STARFM and STAARCH approach need one and more Landsat and MODIS image pair at the same acquisition dates in additional to the target MODIS date. They allow fusing medium spatial resolution data from Landsat with high temporal resolution data from MODIS even surface land types changed. The STARFM and STAARCH approach use surface reflectance data as inputs and require input image pairs (Landsat and MODIS) are consistent and comparable [34, 35]. The generalized reference-based approach accepts DN, TOA reflectance or surface reflectance as input and normalizes input to reference-like data (MODIS-like surface reflectance in this paper). The normalized MODIS-like surface reflectance from multiple medium resolution sensors may be used as inputs for STARFM and STAARCH, which can provide additional input image pairs and thus improve data fusion accuracy. We will further explore this in the near future.

There are two additional advantages associated with using MODIS surface reflectance as reference. First, the MODIS-like surface reflectance provides a way to standardize surface reflectance from different medium resolution sensors to one "standard" and thus allow consistent time-series analysis. Our test on the ASTER, TM, ETM+ and AWiFS data shows they can be combined to form a consistent medium spatial resolution time-series by using MODIS surface reflectance as a reference data set. Second, in theory, MODIS-like medium resolution surface reflectance data may be used to retrieve biophysical parameters for medium resolution data using MODIS algorithm directly and thus take advantages of the knowledge, experiences and lessons learned from MODIS product development. Other consistent coarse resolution data sources can also be used as reference. As we utilize MODIS products as a reference, our results in this paper are limited to the MODIS era.

The accuracy of the general reference-based approach depends on several factors listed below.

(a) data qualities of each medium resolution sensor and MODIS surface reflectance product

The inherent radiometric and geometric qualities of medium resolution sensors will certainly affect the precision with which surface reflectance can be retrieved using either an empirical or physically-based approach. It should be noted, however, that the empirical approach proposed here intrinsically compensates for inaccurate instrument calibration, providing that the relation between DN and radiance is still linear.

(b) intrinsic difference in bandwidth and spectral response function

Differences in spectral bandwidths and spectral response functions may alter the relationship between medium resolution DN and MODIS surface reflectance. We assume that the transformation of response functions between two sensors can be linked linearly. Therefore, the intrinsic difference in bandwidth has been accounted in the transformation. Additional investigation of intrinsic differences may be needed for specific sensors.

(c) accuracy of matching samples from two images

This factor is determined by the sensors' geolocation accuracy and resampling strategy. The aggregated coarse resolution images can provide better location matching samples than fine resolution images as the ratio of geolocation error to pixel size decreases. However, coarse resolution samples reduce data dynamic range when aggregating from fine resolution to coarse resolution and thus average the spectral signals associated with "pure" surface types.

(d) data range and distribution of samples

Well distributed high-quality samples across the full range of DN values can help to reduce the variability about the linear transform.

(e) accuracy of cloud mask from two images

The selected samples must be cloud clear from both images. The MODIS cloud information can be extracted from MODIS product. We define cloud mask for medium

resolution images manually in this paper. An accurate automatic cloud and shadow detection algorithm for the medium resolution data is needed for automatic processing.

(f) spatial variation of aerosol optical depth

The spatial variation of atmospheric condition especially aerosol optical loading may alter the relation between DN values and surface reflectance. The variation of aerosol loading can be partially addressed in the unsupervised classification process by assigning different clusters for a land cover type with different aerosol conditions. Additional aerosol information from other sensors or image itself may be used to improve results. We will further explore this approach for the imagery with spatially variable aerosol loadings.

Acknowledgments

This work was supported by the US Geological Survey (USGS) Landsat Data Continuity Mission (LDCM) Science Team program and the NASA Earth Observing System (EOS) program. Authors would like to thank Robert Tetrault and Bradley Doorn from USDA FAS for providing AWIFS for this paper.

References

[1] W. B. Cohen and S. N. Goward, "Landsat's role in ecological applications of remote sensing," *BioSci.* **54**, 535-545 (2004) [doi:10.1641/0006-3568(2004)054[0535:LRIEAO]2.0.CO;2].

[2] J. C. Townshend, C. O. Justice, W. Li, C. Gurney, and J. McManus, "Global land cover classification by remote sensing: present capabilities and future possibilities," *Rem. Sens. Environ.* **35**, 243-255 (1991) [doi:10.1016/0034-4257(91)90016-Y].

[3] T. R. Loveland and D. M. Shaw, "Multi-resolution land characterization: building collaborative partnerships, in GAP Analysis: A Landscape Approach to Biodiversity Planning," In *Am. Soc. Photogramm. Rem. Sens.*, J. M. Scott, T. H. Tear, and F. W. Davis, Ed., pp. 79-85, Bethesda, MD(1996).

[4] R. Navalgund, "Resourcesat-1 (IRS-P6) - the latest Indian Earth Observation Satellite," *Int. Soc. Photogramm. Rem. Sens. Highlight* **9**, 58-60 (2004).

[5] H. Wang, S. Wang, W. Ma, and T. He, "Development and operation of the IRMSS and CCD camera for CBERS," *Proc. SPIE* **4130**, 9-12 (2002).

[6] M. Abrams, "The Advanced Spaceborne Thermal Emission and Reflection Radiometer (ASTER): data products for the high spatial resolution imager on NASA's Terra plat-form," *Int. J. Remote Sens.* **21**, 847-859 (2000) [doi:10.1080/014311600210326].

[7] M. A. Wulder, J. C. White, S. N. Goward, J. G. Masek, J. R. Irons, M. Herold, W. B. Cohen, T. R. Loveland, and C. E. Woodcock, "Landsat continuity: Issues and opportunities for land cover monitoring," *Rem. Sens. Environ.* **112**, 955-969 (2008) [doi:10.1016/j.rse.2007.07.004].

[8] S. L. Powell, D. Pflugmacher, A. A. Kirschbaum, Y. Kim, and W. B. Cohen, "Moderate resolution remote sensing alternatives: a review of Landsat-like sensors and their applications," *J. Appl. Rem. Sens.* **1**, 012506 (2007) [doi:10.1117/1.2819342].

[9] C. Song, C. E. Woodcock, C. K. Seto, M. P. Lenney, and A. S. Macomber, "Classification and change detection using Landsat TM data: When and how to correct atmospheric effects?" *Rem. Sens. Environ.* **75**, 230-244 (2001) [doi:10.1016/S0034-4257(00)00169-3].

[10] J. G. Masek, E. F. Vermote, N. E. Saleous, R. Wolfe, F. G. Hall, F. Huemmrich, F. Gao, J. Kutler, and T. K. Lim, "A Landsat surface reflectance data set for North America, 1990-2000," *IEEE Geosci. Rem. Sens. Lett.* **3**, 69-72 (2006) [doi:10.1109/LGRS.2005.857030].

[11] Y. J. Kaufman and C. Sendra, "Algorithm for automatic corrections to visible and near-IR satellite imagery," *Int. J. Rem. Sens.* **9**, 1357–1381 (1988) [doi:10.1080/01431168808954942].
[12] J. R. Schott, C. Salvaggio, and W. J. Volchock, "Radiometric scene normalization using pseudo invariant features," *Rem. Sens. Environ.* **26**, 1 – 16 (1988) [doi:10.1016/0034-4257(88)90116-2].
[13] F. G. Hall, D. E. Strebel, J. E. Nickeson, and S. J. Goets, "Radiometric rectification: toward a common radiometric response among multidate, multisensor images," *Rem. Sens. Environ.* **35**, 11–27 (1991) [doi:10.1016/0034-4257(91)90062-B].
[14] Y. Du, J. Cihlar, J. Beaubien, and R. Latifovic, "Radiometric normalization, compositing, and quality control for satellite high resolution image mosaics over large areas," *IEEE Trans. Geosci. Rem. Sens.* **39**, 623–634 (2001) [doi:10.1109/36.911119].
[15] T. A. Schroeder, W. B. Cohen, C. Song, M. J. Canty, Z. Yang, "Radiometric correction of multi-temporal Landsat data for characterization of early successional forest patterns in western Oregon," *Rem. Sens. Environ.* **103**, 16-26 (2006) [doi:10.1016/j.rse.2006.03.008].
[16] I. Olthof, D. Pouliot, R. Fernandes, and R. Latifovic, "Landsat ETM+ radiometric normalization comparison for northern mapping applications," *Rem. Sens. Environ.* **95**, 388-398 (2005) [doi:10.1016/j.rse.2004.06.024].
[17] Y. J. Kaufman, A. Wald, L. A. Remer, B. Gao, R. Li, and L. Flynn, "The MODIS 2.1 lm channel—correlation with visible reflectance for use in remote sensing of aerosol," *IEEE Trans. Geosci. Rem. Sens.* **35**, 1–13 (1997) [doi:10.1109/36.628795].
[18] E. F. Vermote, N. El Saleous, and C. O. Justice, "Atmospheric correction of the MODIS data in the visible to middle infrared: First results," *Rem. Sens. Environ.* **83**, 97-111 (2002) [doi:10.1016/S0034-4257(02)00089-5].
[19] S. Liang, H. Fang, M. Chen, C. Walthall, C. Daughtry, J. Morisette, C. Schaaf, and A. Strahler, "Validating MODIS land surface reflectance and albedo products: Methods and preliminary results," *Rem. Sens. Environ.* **83**(1-2), 149-162 (2002) [doi:10.1016/S0034-4257(02)00092-5].
[20] MODIS Land Surface Reflectance Web site, URL: http://modis-sr.ltdri.org/MAIN_VALIDATION/UNCERTAINTY_1.html
[21] W. H. Press, S. A. Teukolsky, W. T. Vetterling, and B. P. Flannery, *Numerical Recipes 3rd Edition: The Art of Scientific Computing*, pp. 785-787, Cambridge University Press (2007).
[22] C. O. Justice, J. R. G. Townshend, E. F. Vermote, E. Masuoka, R. E. Wolfe, N. Saleous, D. P. Roy, and J. T. Morisette, "An overview of MODIS land processing and products status," *Rem. Sens. Environ.* **83**, 3-15 (2002) [doi:10.1016/S0034-4257(02)00084-6].
[23] J. T. Morisette, J. L. Privette, and C. O. Justice, "A framework for the validation of MODIS Land products," *Rem. Sens. Environ.* **83**, 77-96 (2002) [doi:10.1016/S0034-4257(02)00088-3].
[24] C. B. Schaaf, F. Gao, A. H. Strahler, W. Lucht, X. Li, T. Tsang, N. C. Strugnell, X. Zhang, Y. Jin, J. -P. Muller, P. Lewis, M. Barnsley, P. Hobson, M. Disney, G. Roberts, M. Dunderdale, C. Doll, R. d'Entremont, B. Hu, S. Liang, J. L. Privette, and D. P. Roy, "First Operational BRDF, albedo and ndir reflectance products from MODIS," *Rem. Sens. Environ.* **83**, 135-148 (2002) [doi:10.1016/S0034-4257(02)00091-3].
[25] Y. Jin, C. B. Schaaf, C. E. Woodcock, F. Gao, X. Li, A. H. Strahler, W. Lucht, and S. Liang, "Consistency of MODIS surface BRDF/albedo retrievals: 2. validation," *J. Geophy. Res.* **108**(D5), 4159 (2003) [doi:10.1029/2002JD002804].

[26] M. A. Friedl, D. K. McIver, J. C. F. Hodges, X. Zhang, D. Muchoney, A. H. Strahler, C. E. Woodcock, S. Gopal, A. Schnieder, A. Cooper, A. Baccini, F. Gao, and C. B. Schaaf, "Global land cover mapping from MODIS: algorithms and early results," *Rem. Sens. Environ.* **83**, 287-302 (2002) [doi:10.1016/S0034-4257(02)00078-0].

[27] J. K. Ross, *The Radiation Regime and Architecture of Plant Stands*, 392 pp., Dr. W. Junk Publishers, The Netherlands (1981).

[28] X. Li and A. H. Strahler, "Geometric-optical bidirectional reflectance modeling of a conifer forest canopy," *IEEE Trans. Geosci. Rem. Sens.* **24**, 906-919 (1986) [doi:10.1109/TGRS.1986.289706].

[29] W. Lucht, C. B. Schaaf, and A. H. Strahler, "An algorithm for the retrieval of albedo from space using semiempirical BRDF models," *IEEE Trans. Geosci. Rem. Sens.* **38**, 977-998 (2000) [doi:10.1109/36.841980].

[30] National Remote Sensing Agency (NRSA), "IRS-P6 Data User's Manual, 142 pp. (2003).

[31] U. S. Department of Agriculture (USDA) National Agricultural Statistics Service (NASS) http://www.nass.usda.gov/research/Cropland/SARS1a.html

[32] G. Chander, M. J. Coan, and P. L. Scaramuzza, "Evaluation and comparison of the IRS-P6 and the Landsat sensors," *IEEE Trans. Geosci. Rem. Sens.* **46**(1), 209–221 (2008) [doi:10.1109/TGRS.2007.907426].

[33] D. P. Roy, J. Ju, K. Kline, P. L. Scaramuzza, V. Kovalskyy, M. Hansen, T. R. Loveland, E. Vermote, and C. Zhang, "Web-enabled Landsat Data (WELD): Landsat ETM+ composited mosaics of the conterminous United States," *Rem. Sens. Environ.* **114**, 35–49 (2010) [doi: 10.1016/j.rse.2009.08.011].

[34] F. Gao, J. Masek, M. Schwaller and F. Hall, "On the Blending of the Landsat and MODIS Surface Reflectance: Predict Daily Landsat Surface Reflectance," *IEEE Trans. Geosci. Rem. Sens.*, **44**, 2207-2218 (2006) [doi:10.1109/TGRS.2006.872081].

[35] T. Hilker, M. A. Wulder, N. C. Coops, J. Linke, G. McDermid, J. G. Masek, F. Gao, and J. C. White, "A new data fusion model for high spatial- and temporal- resolution mapping of forest disturbance based on Landsat and MODIS," *Rem. Sens. Environ.* (2009) [doi:10.1016/j.rse.2009.03.007].